© 2016. Published by The Company of Biologists Ltd | Journal of Cell Science (2016) 129, 1940-1949 doi:10.1242/jcs.182220

RESEARCH ARTICLE

The Mg^{2+} transporter CNNM4 regulates sperm Ca^{2+} homeostasis and is essential for reproduction

Daisuke Yamazaki[1], Haruhiko Miyata[2], Yosuke Funato[1], Yoshitaka Fujihara[2], Masahito Ikawa[2] and Hiroaki Miki[1,*]

ABSTRACT

Ca^{2+} influx triggers sperm capacitation; however, the underlying regulatory mechanisms remain incompletely understood. Here, we show that CNNM4, a Mg^{2+} transporter, is required for Ca^{2+} influx during capacitation. We find that *Cnnm4*-deficient male mice are almost infertile because of sperm dysfunction. Motion analyses show that hyperactivation, a qualitative change in the mode of sperm motility during capacitation, is abrogated in *Cnnm4*-deficient sperm. In contrast, tyrosine phosphorylation of flagellar proteins, a hallmark of capacitation, is excessively augmented. These seemingly paradoxical phenotypes of *Cnnm4*-deficient sperm are very similar to those of sperm lacking a functional cation channel of sperm (CatSper) channel, which plays an essential role in Ca^{2+} influx during sperm capacitation. Ca^{2+} imaging analyses demonstrate that Ca^{2+} influx is perturbed in *Cnnm4*-deficient sperm, and forced Ca^{2+} entry into these sperm normalizes the level of tyrosine phosphorylation. Furthermore, we confirm the importance of CNNM4 in sperm by generating germ-cell-specific *Cnnm4*-deficient mice. These results suggest a new role of CNNM4 in sperm Ca^{2+} homeostasis.

KEY WORDS: Sperm capacitation, Calcium, Hyperactivation, CNNM4

INTRODUCTION

Sperm are maintained in an immotile state in the epididymis and start swimming after ejaculation into the female reproductive tract. However, they are incapable of fertilizing eggs immediately after ejaculation and undergo several qualitative changes (collectively referred to as capacitation) to become competent for fertilization (Austin, 1951, 1952; Chang, 1951). One of the visible events occurring during capacitation is a change in the mode of flagellar beating. Freshly ejaculated sperm show a nearly symmetrical flagellar beat pattern, whereas capacitated sperm show an increased amplitude of flagellar bend and asymmetrical flagellar beating. These changes are called hyperactivation and provide a driving force for sperm to swim through environments of relatively high viscosity (Suarez, 2008), such as the oviduct and zona pellucida, a glycoprotein layer surrounding the egg.

Capacitation involves several biochemical changes, such as increase in the levels of intracellular pH (pH_i), Ca^{2+} ($[Ca^{2+}]_i$), and cAMP, and tyrosine phosphorylation of flagellar proteins (Darszon et al., 2011; Lishko et al., 2012). Media used for the capacitation of sperm *in vitro* commonly contain three key components: HCO_3^-, Ca^{2+} and bovine serum albumin (BSA) (Yanagimachi, 1994). An increase in $[Ca^{2+}]_i$ plays a central role in sperm capacitation (Darszon et al., 2011; Lishko et al., 2012), and both HCO_3^- and BSA are involved in Ca^{2+} entry into sperm. When epididymal sperm are released into the capacitation medium, HCO_3^- enters the sperm through a Na^+/HCO_3^- co-transporter (Demarco et al., 2003) and activates soluble adenylyl cyclase, which increases intracellular cAMP levels (Chen et al., 2000). Elevated cAMP levels activate protein kinase A (PKA) signaling, which is followed by the influx of extracellular Ca^{2+} (Tateno et al., 2013) and tyrosine phosphorylation of flagellar proteins (Visconti et al., 1995). Application of HCO_3^- to sperm elicits an increase in pH_i (Demarco et al., 2003), and artificial elevation of pH_i by itself can induce Ca^{2+} influx into sperm (Santi et al., 1998). Thus, HCO_3^- stimulates Ca^{2+} entry into sperm through the control of cAMP–PKA pathway and pH_i. BSA is also needed for the entry of extracellular Ca^{2+} into sperm (Espinosa et al., 2000), but the mechanism of how BSA functions in this process is still ambiguous. HCO_3^--stimulated PKA activation did not proceed in the absence of BSA (Osheroff et al., 1999; Visconti et al., 1999), indicating that BSA plays an essential role in HCO_3^-–cAMP–PKA pathway activation. Given that this pathway leads to Ca^{2+} influx through the control of pH_i, BSA can be considered to contribute to Ca^{2+} influx through control of this pathway. However, there is a report that BSA is also involved in Ca^{2+} influx in a manner independent of pH_i change (Xia and Ren, 2009a), and thus, BSA appears to have an additional role in Ca^{2+} influx, besides HCO_3^-–cAMP–PKA pathway activation.

Cation channel of sperm (CatSper) channel mediates Ca^{2+} influx into sperm (Ren and Xia, 2010), which is essential for capacitation as described above. The CatSper channel complex contains four pore-forming α subunits (CatSper1–CatSper4) and three auxiliary subunits (CatSperβ, CatSperγ, and CatSperδ) (Chung et al., 2011; Liu et al., 2007; Qi et al., 2007; Wang et al., 2009). Male mice lacking each of *CatSper1–CatSper4* and *CatSperd* are infertile and their sperm show defects in Ca^{2+} influx and hyperactivation during *in vitro* capacitation experiments (Carlson et al., 2005; Chung et al., 2011; Qi et al., 2007; Quill et al., 2003; Ren et al., 2001) indicating that CatSper-dependent Ca^{2+} influx is essential for hyperactivation. In *in vitro* fertilization (IVF) assays, *CatSper*-deficient sperm can fertilize the eggs only when the zona pellucida has been enzymatically removed (Quill et al., 2003; Ren et al., 2001), which is consistent with the importance of hyperactivated motility for penetrating the zona pellucida. A recent study reported excessive tyrosine phosphorylation of flagellar proteins in *CatSper1*-deficient sperm stimulated with the capacitation medium, suggesting a role for CatSper-dependent Ca^{2+} influx in suppressing and normalizing the level of tyrosine phosphorylation (Chung et al., 2014). The above data collectively indicate the importance of the CatSper channel in capacitation. Several stimuli such as cyclic nucleotides, alkaline depolarization, BSA and zona pellucida glycoproteins induce CatSper-dependent Ca^{2+} influx (Ren et al., 2001; Xia and

[1]Department of Cellular Regulation, Research Institute for Microbial Diseases, Osaka University, 3-1 Yamadaoka, Suita, Osaka 565-0871, Japan. [2]Department of Experimental Genome Research, Research Institute for Microbial Diseases, Osaka University, 3-1 Yamadaoka, Suita, Osaka 565-0871, Japan.

*Author for correspondence (hmiki@biken.osaka-u.ac.jp)

Received 19 October 2015; Accepted 15 March 2016

Journal of Cell Science (2016) 129, 1940-1949 doi:10.1242/jcs.182220

Ren, 2009a,b; Xia et al., 2007), but there remain many unsolved problems regarding the regulatory and functional mechanisms of the CatSper channel (Ren and Xia, 2010).

In this study, we generated and analyzed mice lacking *Cnnm4*, which encodes cyclin M4 (CNNM4, also known as ancient conserved domain protein 4), a membrane protein, and observed that *Cnnm4*-deficient male mice showed severely impaired fertility. CNNM4 localizes at the basolateral membrane of the intestinal epithelia and mediates transcellular Mg^{2+} transport (Yamazaki et al., 2013), but the function of CNNM4 in non-epithelial cells remains unknown. CNNM4 is expressed in the sperm, and detailed functional analyses of *Cnnm4*-deficient sperm showed an unexpected role of CNNM4 in sperm Ca^{2+} homeostasis.

RESULTS

Cnnm4-deficient male mice are almost infertile

In our previous study (Yamazaki et al., 2013), we generated mice carrying a mutant *Cnnm4*$^{-}$ allele, containing a splice acceptor in an intron before exon 2 of *Cnnm4*. Immunoblotting analyses could not detect CNNM4 expression in *Cnnm4*$^{-/-}$ mice; however, presence of an expression leak could not be denied. To disrupt *Cnnm4* completely, exons 2–5, which encode functionally essential cystathionine-β-synthase domains (Hirata et al., 2014), were deleted using the Cre-loxP system. The resultant allele is referred to as *Cnnm4*$^{\Delta}$ (Fig. S1). *Cnnm4*$^{\Delta/\Delta}$ mice were viable and showed no gross abnormalities. *Cnnm4*$^{\Delta/\Delta}$ female mice showed normal copulatory behavior when mated with wild-type male mice, and produced offspring that were comparable to those produced by wild-type female mice (*Cnnm4*$^{+/+}$, 7.0±1.0 pups; *Cnnm4*$^{\Delta/\Delta}$, 6.5±0.7 pups; mean±s.e.m.; n=6 for each genotype, P>0.05). In contrast, mating of *Cnnm4*$^{\Delta/\Delta}$ male mice with wild-type female mice greatly decreased pregnancy rate and the number of offspring born (Fig. 1A). These observations indicate the importance of CNNM4 in male fertility.

Our previous study has shown that CNNM4 is highly expressed in the testis (Yamazaki et al., 2013). Histological analyses of the testis and epididymis isolated from *Cnnm4*$^{\Delta/\Delta}$ mice showed no obvious differences (Fig. 1B). Moreover, the lumen of the duct in the epididymal caput and cauda of *Cnnm4*$^{\Delta/\Delta}$ mice was filled with sperm, which was similar to that observed in wild-type mice (Fig. 1B). Furthermore, cauda epididymal sperm isolated from *Cnnm4*$^{\Delta/\Delta}$ mice were morphologically normal (Fig. 1C), and their number in the proximal vas deferens was not significantly altered (*Cnnm4*$^{+/+}$, $6.8\times10^5\pm1.1\times10^5$; *Cnnm4*$^{\Delta/\Delta}$, $7.4\times10^5\pm0.8\times10^5$; mean±s.e.m.; n=10 for each genotype, P>0.05), suggesting that spermatogenesis was not grossly affected in *Cnnm4*$^{\Delta/\Delta}$ mice.

Immunoblotting analyses of lysates obtained from male reproductive organs and sperm showed that CNNM4 was expressed in the testis, epididymis, and sperm (Fig. 2A). *Cnnm* genes are highly conserved through evolution (Wang et al., 2003), and it remains unknown whether these genes are generally expressed in male germ cells in divergent organisms. However, we confirmed the expression of CNNM4 at least in human sperm (Fig. 2B). The *Cnnm4*$^{\Delta}$ allele had a tandemly aligned set of internal ribosome entry sites (IRES) and a β-galactosidase reporter gene to allow visual determination of *Cnnm4* expression (Fig. S1A). β-Galactosidase staining of testicular germ cells and sperm with X-gal yielded positive signals (Fig. 2C), indicating that *Cnnm4* was expressed in germ line cells. Epithelial cells from the epididymis also yielded positive results for β-galactosidase staining. Direct staining of sperm isolated from the cauda epididymis for CNNM4 yielded strong non-specific signals in the mid-piece area and clear specific signals in the principal piece of sperm tail (Fig. 2D). CNNM4 signals in the principal piece disappeared when the anti-CNNM4 antibody was pre-incubated with its antigen peptide (Fig. S2). We physically separated the sperm tail from the head and performed immunoblotting analysis, which confirmed that CNNM4 was exclusively expressed in the sperm tail (Fig. 2E).

Cnnm4-deficient sperm show impaired fertilizing ability and motility

Because we did not observe obvious abnormalities in spermatogenesis in *Cnnm4*$^{\Delta/\Delta}$ mice, we examined the function of sperm isolated from these mice. We performed IVF assays to investigate the fertilizing ability of these sperm. When *Cnnm4*-deficient sperm were incubated with cumulus-free zona-pellucida-intact eggs, no eggs progressed to the two-cell stage (Fig. 3A,B). We enzymatically removed the zona pellucida to eliminate obstruction during sperm penetration. Because polyspermy affects egg development (Wortzman-Show et al., 2007), we counted the number of eggs showing pronuclear formation as an indicator for fertilization (Fig. 3C). We observed that *Cnnm4*-deficient sperm could fertilize zona-pellucida-free eggs, although the efficiency of fertilization was lower than that observed with wild-type sperm (Fig. 3D). *Cnnm4*-deficient sperm could bind to the zona-pellucida-intact eggs as wild-type sperm (Fig. 3E). These results suggest that the

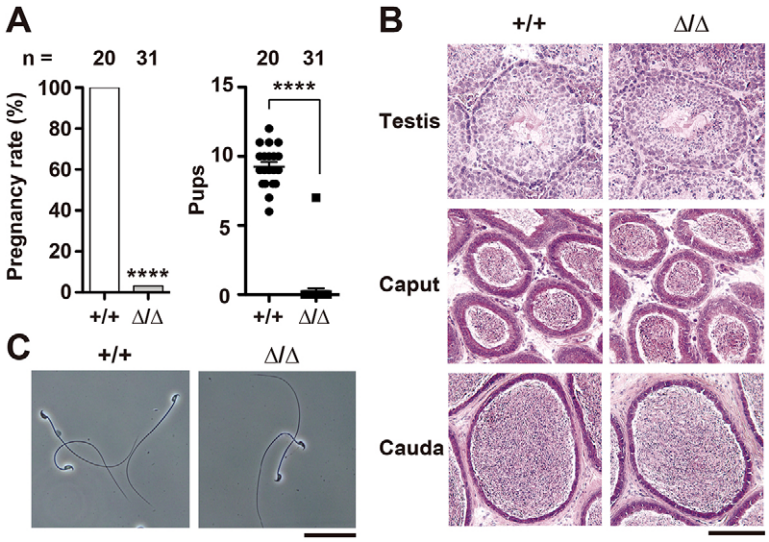

Fig. 1. *Cnnm4*-deficient male mice are impaired in fertility. (A) 2- to 3-month-old *Cnnm4*$^{+/+}$ and *Cnnm4*$^{\Delta/\Delta}$ male mice were mated with wild-type female mice for 3 months. Female mice that produced one or more pups were considered pregnant. Left, pregnancy rate (pregnancy/vaginal plug formation) is expressed as a percentage. Right, each data point represents an individual number of offspring. Black bars indicate the mean±s.e.m. ****P<0.0001 (chi-squared test, left; two-tailed Student's t-test, right). The total number of vaginal plug-positive female mice analyzed is shown above each bar. (B) Sections of the testis and epididymis were stained with H&E. Scale bar: 100 µm. (C) Phase-contrast images of sperm isolated from the cauda epididymis. Scale bar: 50 µm.

Journal of Cell Science (2016) 129, 1940-1949 doi:10.1242/jcs.182220

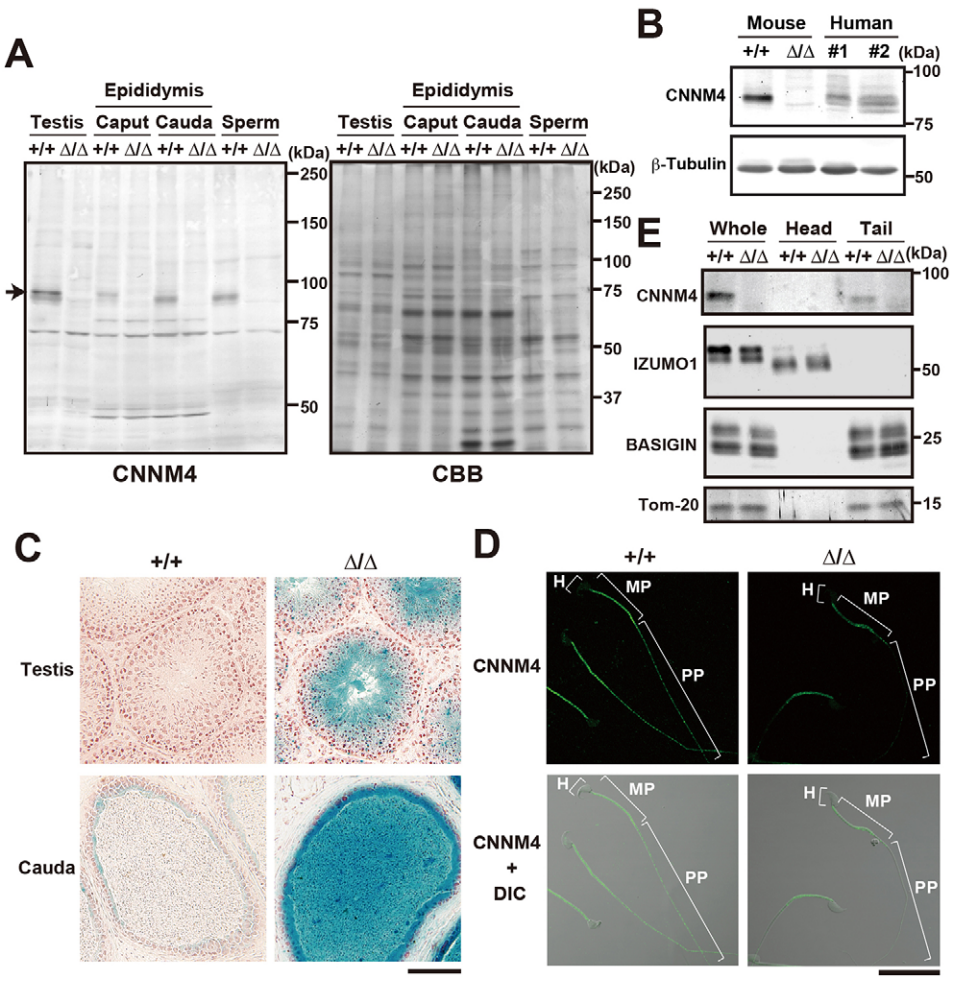

Fig. 2. CNNM4 expression in the testis, epididymis and sperm. (A) Lysates of the testis, epididymis and sperm were immunoblotted with anti-CNNM4 antibody. An arrow indicates CNNM4. Coomassie-stained images (CBB) are also indicated. (B) Lysates of mouse sperm from *Cnnm4*$^{+/+}$ and *Cnnm4*$^{\Delta/\Delta}$ mice and of human sperm from two fertile donors were immunoblotted with anti-CNNM4 and -β-tubulin antibodies, respectively. (C) Cryosections of the testis and cauda epididymis of 3-month-old *Cnnm4*$^{+/+}$ and *Cnnm4*$^{\Delta/\Delta}$ mice were subjected to β-galactosidase staining (counterstained with Neutral Red). Scale bar: 100 µm. (D) Sperm isolated from the cauda epididymis were analyzed by performing immunofluorescence staining with anti-CNNM4 antibody (green). Differential interference contrast images are also indicated. H, head; MP, mid-piece; PP, principal piece. Scale bar: 20 µm. (E) The heads and tails of sperm were separated by sonication, and their lysates were immunoblotted with the indicated antibody. IZUMO1 (localized in the head), BASIGIN (in the tail), and Tom-20 (in the mid-piece) were used as separation controls.

ability to penetrate the zona pellucida is impaired in *Cnnm4*-deficient sperm.

Next, we examined the motility of *Cnnm4*-deficient sperm by performing computer-assisted sperm analysis (CASA). Cauda epididymal sperm were incubated in conventional capacitation medium, and their percentage motility was measured every 2 h for 6 h. The percentage motility of wild-type sperm was constant for 6 h but that of *Cnnm4*-deficient sperm decreased gradually to 6.5% after 6 h (Fig. 4A). All parameters associated with the speed of sperm motility, i.e. path, linear and track velocities, were moderately reduced in *Cnnm4*-deficient sperm (Fig. 4B).

During capacitation, sperm motility is hyperactivated, which is considered to allow the sperm to penetrate through environments of relatively high viscosity, such as the zona pellucida. Therefore, we directly monitored sperm movement by performing negative phase-contrast microscopy to visualize the flagella. Both wild-type and *Cnnm4*-deficient sperm moved in a similar manner immediately after their release into the capacitation medium (Movie 1, wild-type; Movie 2, *Cnnm4*-deficient). After 2 h of incubation in the capacitation medium, wild-type sperm showed striking changes in the mode of motility, including asymmetrical flagellar movement and increased bending amplitude (Movie 3; Fig. 4C, left). However, these mode changes were not observed in *Cnnm4*-deficient sperm (Movie 4; Fig. 4C, right). To quantitatively assess this phenomenon, the maximum bend angle of the mid-piece of each sperm was measured (Carlson et al., 2005; Chung et al., 2011). We observed that the maximum bend angle became larger after capacitation in wild-type sperm (Fig. 4D), as reported previously (Carlson et al., 2005). However, no significant change was observed in the maximum bend angle of *Cnnm4*-deficient sperm even after incubation in the capacitation medium for the same time period (Fig. 4D). These results indicated that CNNM4 deficiency abrogated sperm motility and hyperactivation.

Germ cell-specific *Cnnm4* deficiency impairs sperm motility

In male reproductive organs, CNNM4 is expressed in both germ cells and epididymal epithelial cells (Fig. 2C). To confirm the significance of CNNM4 in germ cells, we generated conditional knockout *Cnnm4*$^{flox/\Delta}$;*Stra8-Cre* mice harboring inactivated *Cnnm4* that was produced by deleting exons 2–5 in male germ cells using a *Stra8* promoter (Fig. S3) (Sadate-Ngatchou et al., 2008). CNNM4 expression was barely detectable in the testis and sperm of these mice (Fig. S4A), indicating that Cre-mediated deletion of *Cnnm4* occurred in the majority of germ cells. Sperm obtained from *Cnnm4*$^{flox/\Delta}$;*Stra8-Cre* mice showed decreased percentage motility and speed of motility, and no hyperactivation (Fig. S4B–D), which was similar to that observed in *Cnnm4*-deficient sperm. These results confirmed the importance of CNNM4 in germ cells in regulating sperm motility.

Cnnm4-deficient sperm show excessive tyrosine phosphorylation

Decreased motility and defective hyperactivation observed in *Cnnm4*-deficient sperm suggested abnormal capacitation. To

Journal of Cell Science (2016) 129, 1940-1949 doi:10.1242/jcs.182220

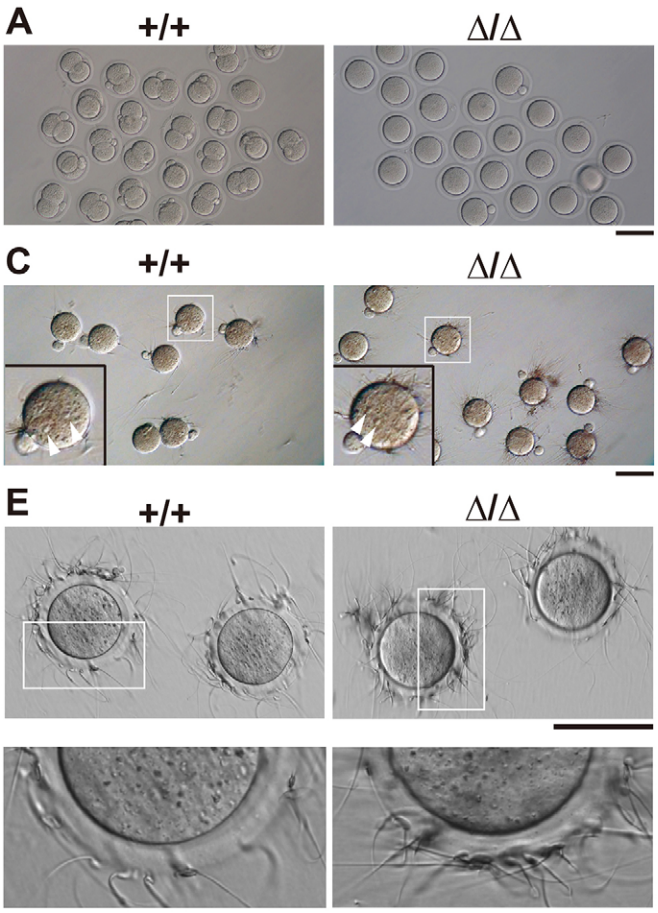

Fig. 3. IVF experiments. (A) Differential-interference-contrast images of zona-pellucida-intact eggs 24 h after incubation with sperm isolated from 6-month-old *Cnnm4*$^{+/+}$ and *Cnnm4*$^{Δ/Δ}$ mice. Scale bar: 100 µm. (B) IVF rates of sperm with zona-pellucida-intact eggs. Data are expressed as mean±s.e.m. of four independent experiments. The total number of eggs analyzed is shown above each bar. (C) Differential-interference-contrast images of zona-pellucida-free eggs 8 h after incubation with sperm. Magnified images of the boxed areas are also indicated at the bottom left. Arrowheads indicate the pronucleus. Scale bar: 100 µm. (D) IVF rates of sperm with zona-pellucida-free eggs. Data are expressed as mean± s.e.m. of five independent experiments. The total number of eggs analyzed is shown above each bar. ****P<0.0001 (chi-squared test). (E) Differential-interference-contrast images of zona-pellucida-intact eggs incubated with sperm for 30 min. Magnified images of the boxed areas are also shown at the bottom. Scale bar: 100 µm.

investigate whether capacitation-associated changes in intracellular signaling were altered in *Cnnm4*-deficient sperm, we determined the status of tyrosine phosphorylation, a hallmark of capacitation (Visconti et al., 1995), in these sperm. Wild-type sperm showed an increase in tyrosine phosphorylation under the capacitation medium (Fig. 5A). Unexpectedly, phosphorylation signals were much stronger in *Cnnm4*-deficient sperm than in wild-type sperm (Fig. 5A). Such excessive tyrosine phosphorylation was also observed to occur in germ-cell-specific *Cnnm4*-deficient sperm (Fig. 5A). Results of immunostaining indicated that tyrosine phosphorylation of flagellar proteins occurred earlier in *Cnnm4*-deficient sperm than in wild-type sperm (Fig. 5B). These results indicate that CNNM4 deficiency abnormally stimulated the tyrosine phosphorylation of flagellar proteins.

CatSper1, a pore-forming subunit of the CatSper channel, is essential for sperm hyperactivation, and loss of *CatSper1* results in excessive tyrosine phosphorylation of flagellar proteins (Chung et al., 2014). Influx of extracellular Ca^{2+} through the CatSper channel is required for the normal regulation of tyrosine phosphorylation during sperm capacitation. To examine whether forced Ca^{2+} entry repressed excessive tyrosine phosphorylation in *Cnnm4*-deficient sperm, we incubated these sperm in the capacitation medium supplemented with Ca^{2+} ionophore A23187. Treatment with A23187 decreased and normalized the level of tyrosine phosphorylation in *Cnnm4*-deficient sperm (Fig. 5C). Moreover, this decrease required extracellular Ca^{2+} present in the medium (Fig. 5D). These results suggest that CNNM4 deficiency impairs Ca^{2+} influx in sperm.

Cnnm4-deficient sperm show impaired Ca^{2+} influx

CatSper-dependent Ca^{2+} influx during capacitation occurs very rapidly (within 5 s) (Xia and Ren, 2009a; Xia et al., 2007). To investigate this, we performed Ca^{2+} imaging analyses with Fluo-4 by artificially initiating capacitation by adding BSA, an essential ingredient of the capacitation medium, and monitoring the response of sperm. Stimulation of wild-type sperm first produced an increase of fluorescence signals in the tail region, which then spread toward the head region (Fig. 6A), as reported previously (Xia and Ren, 2009a; Xia et al., 2007). In contrast, stimulation of *Cnnm4*-deficient sperm with BSA produced a very small increase of fluorescence signals (Fig. 6A). Quantification of fluorescence signals in the head region indicated a significant suppression of BSA-stimulated increase in Ca^{2+} influx in *Cnnm4*-deficient sperm (Fig. 6B,C). These results established the importance of CNNM4 in Ca^{2+} influx during capacitation. We examined the presence of CatSper1 in sperm, but immunoblotting analyses showed no decrease of CatSper1 in *Cnnm4*-deficient sperm (Fig. 6D).

CNNM4 regulates Mg^{2+} levels in sperm

CNNM4 stimulates Mg^{2+} efflux in epithelial cells (Yamazaki et al., 2013; Funato et al., 2014). Therefore, we measured Mg^{2+} levels in sperm using inductively coupled plasma mass spectrometry (ICP-MS). As shown in Fig. 7A, Mg^{2+} levels were significantly increased in *Cnnm4*-deficient sperm, whereas Ca^{2+} levels were not affected. Based on these results, we hypothesized that too much Mg^{2+} in sperm caused by *Cnnm4* deficiency abrogates sperm motility and hyperactivation. Therefore, we examined the effect of changing the concentration of Mg^{2+} in the incubation medium. When *Cnnm4*-

Journal of Cell Science (2016) 129, 1940-1949 doi:10.1242/jcs.182220

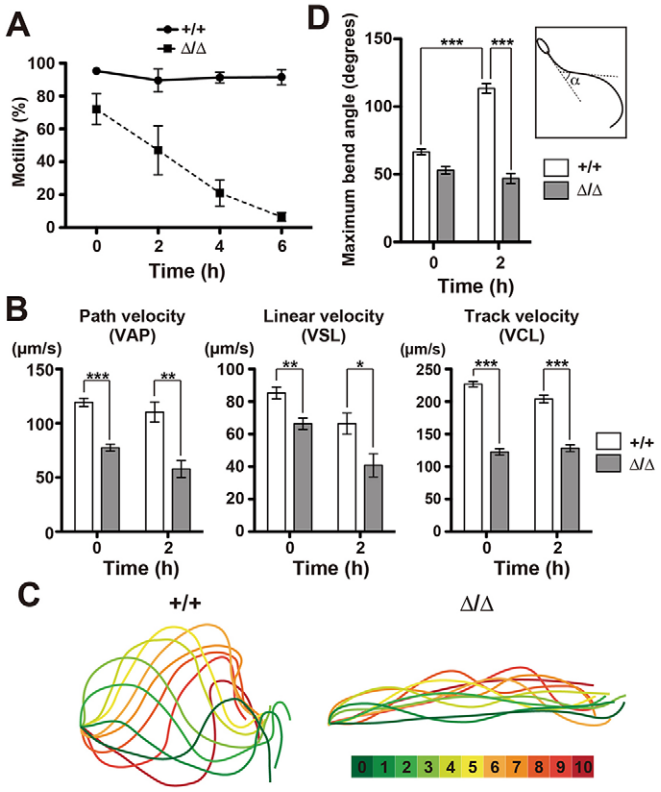

Fig. 4. *Cnnm4*-deficient sperm show decreased motility. (A) Sperm isolated from *Cnnm4*$^{+/+}$ and *Cnnm4*$^{\Delta/\Delta}$ mice were incubated in the Toyoda-Yokoyama-Hoshi (TYH) medium for the indicated time, and their percentage motility was measured using CASA. Data are expressed as mean±s.e.m. Four independent experiments were performed. (B) Sperm were incubated for the indicated time, and their path, linear and track velocities were measured using CASA. Data are expressed as mean±s.e.m. Four independent experiments were performed. **P*<0.05, ***P*<0.01, ****P*<0.001 (two-tailed Student's *t*-test). (C) Representative flagellar waveform traces. After incubating sperm in the TYH medium for 2 h, flagellar waveforms of a single sperm were traced and are shown by using different colors for each frame (from 0 to 10). The time interval between each frame is 15 ms. (D) Sperm were incubated for the indicated time, and the maximum bend angles (inset, α) of the mid-piece were measured. We analyzed 100 sperm from five mice of each genotype (20 sperm from each mouse). Data are expressed as mean±s.e.m. of five independent experiments. ****P*<0.001 (one-way ANOVA with Tukey's multiple comparison test).

deficient sperm were incubated in Mg^{2+}-free medium for 2 h, their percentage motility and maximum bend angle of the mid-piece were restored to 78% and 73°, respectively (Fig. 7B,C). The level of tyrosine phosphorylation of *Cnnm4*-deficient sperm was also decreased in Mg^{2+}-free medium (0 mM) in comparison to the result in the normal medium (1.2 mM) (Fig. 7D). In contrast, when wild-type sperm were incubated in the medium supplemented with 40 mM Mg^{2+}, the increase in the bend angle was completely suppressed (Fig. 7C) and the level of tyrosine phosphorylation was increased to the same level as that of *Cnnm4*-deficient sperm incubated in the normal medium (Fig. 7D). Taken together, regulation of intracellular Mg^{2+} level by CNNM4 appears to be important for sperm motility and hyperactivation.

DISCUSSION

We previously reported that CNNM4 is strongly expressed in the intestine and is involved in Mg^{2+} absorption from digested food (Yamazaki et al., 2013). Indeed, *Cnnm4*$^{-/-}$ mice showed substantial impairment in intestinal Mg^{2+} absorption. However, this defect was counterbalanced by the restricted urinary excretion of Mg^{2+}, and *Cnnm4*$^{-/-}$ mice only showed subtle hypomagnesemia without excessive abnormalities in their development or growth. However, these mice showed defective development of the tooth enamel. Histological analyses indicated a strong and specific expression of CNNM4 in ameloblasts, which are epithelial cells that promote enamel mineralization. In the present study, we observed functional defects in sperm isolated from *Cnnm4*$^{\Delta/\Delta}$ mice, suggesting the importance of CNNM4 in sperm. Our previous study showed that CNNM4 was expressed in the testis (Yamazaki et al., 2013) and the present study showed that CNNM4 was mainly expressed in male germ cells (Fig. 2). Besides germ cells, CNNM4 expression was also observed in epididymal epithelial cells (Fig. 2), and CNNM4 might be involved in the regulation of intraluminal Mg^{2+} concentration in the epididymal duct. Extracellular Mg^{2+} levels affect sperm motility and hyperactivation (Fig. 7), suggesting the possibility that abnormal regulation of Mg^{2+} in the epididymis affects sperm motility in the absence of CNNM4. However, sperm isolated from germ-cell-specific *Cnnm4*-deficient mice (*Cnnm4*$^{flox/\Delta}$;*Stra8-Cre* mice) were phenotypically similar to those from *Cnnm4*$^{\Delta/\Delta}$ mice (Fig. 5A; Fig. S4), confirming that CNNM4 in germ cells was crucial for the normal function of sperm. It should be noted that this new function of CNNM4 in sperm is qualitatively different from its original function. A previous study has indicated that CNNM4 localizes to the basolateral membrane of epithelial cells and mediates the directional transport of Mg^{2+} across the epithelial barrier at the tissue level (Yamazaki et al., 2013). Analyses of sperm clearly showed the importance of CNNM4 in a single cell and indicated that this function was mechanistically different from its function in epithelial cells. Moreover, we showed that Mg^{2+} levels were significantly increased in *Cnnm4*-deficient sperm, and their phenotypes were partially rescued by Mg^{2+} depletion from the medium (Fig. 7). These results suggest that the abnormal elevation of intracellular Mg^{2+} might affect sperm function. At present, it is unclear how the intrinsic Mg^{2+} efflux activity of CNNM4 is associated with sperm function.

Cnnm4-deficient sperm exhibited several abnormalities that were similar to those in sperm lacking a functional CatSper channel (Carlson et al., 2005; Chung et al., 2011, 2014; Qi et al., 2007; Quill et al., 2003; Ren et al., 2001). These sperm were motile but showed severe defects in hyperactivation. In addition, these sperm showed excessive tyrosine phosphorylation of flagellar proteins (Fig. 5). These similarities raise the possibility that there could be a functional relationship between CNNM4 and the CatSper channel. Careful comparison of the results indicated the following differences. First, we observed a reduced but significant Ca^{2+} influx in *Cnnm4*-deficient sperm (Fig. 6), which is in contrast to its complete abolition in sperm with a non-functional CatSper channel. Second, the motility rate of *Cnnm4*-deficient sperm gradually decreased after incubation in the capacitation medium for 6 h (Fig. 4A). However, sperm with a non-functional CatSper channel lose their motility very rapidly, with most sperm ceasing to swim after 90 min of incubation (Qi et al., 2007). In contrast, ∼50% of *Cnnm4*-deficient sperm were motile even after 120 min of incubation. One should be cautious about drawing definitive conclusions based on the comparison of data published in various studies. However, the phenotypes of *Cnnm4*-deficient sperm seem to be less severe than those of sperm with a non-functional CatSper channel. All the other CNNMs (CNNM1–CNNM3) are expressed in the testis (de Baaij et al., 2012; Wang et al., 2004) and thus might compensate for CNNM4 deficiency. More detailed examination of their expression and

Journal of Cell Science (2016) 129, 1940-1949 doi:10.1242/jcs.182220

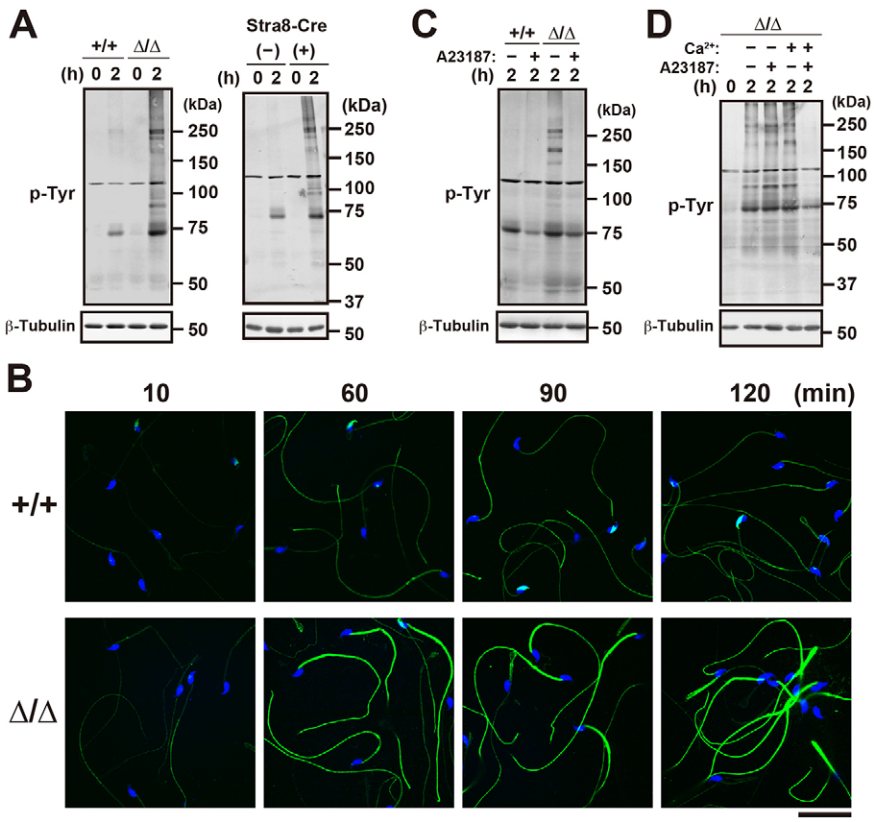

Fig. 5. Capacitation-associated protein tyrosine phosphorylation. (A) Sperm isolated from 3-month-old *Cnnm4*$^{+/+}$, *Cnnm4*$^{\Delta/\Delta}$, *Cnnm4*$^{flox/\Delta}$ (Stra8-Cre –) and *Cnnm4*$^{flox/\Delta}$;*Stra8-Cre* (Stra8-Cre +) mice were incubated in the TYH medium for the indicated time. Lysates of sperm were immunoblotted with anti-phosphotyrosine (p-Tyr) and -β-tubulin antibodies. (B) Sperm were incubated in the TYH medium for the indicated time and were examined by performing immunofluorescence staining with anti-phosphotyrosine antibody (green) and DAPI (blue). Scale bar: 30 µm. (C) Sperm were incubated in the TYH medium with or without 20 µM Ca^{2+} ionophore A23187 for 2 h, and their lysates were immunoblotted. (D) *Cnnm4*-deficient sperm were incubated in the TYH medium for 30 min and were transferred to Ca^{2+}-free or normal TYH medium, followed by incubation with or without 20 µM A23187 for 90 min. Sperm lysates were immunoblotted.

function is needed to clarify this problem. It should be noted that *Cnnm4*-deficient mice were almost infertile, although suppression of the Ca^{2+} influx in their sperm was partial. *Cnnm4*-deficient sperm failed to develop hyperactivated motility and could not fertilize with zona-pellucida-intact eggs, as with *CatSper1*-deficient sperm (Ren et al., 2001; Carlson et al., 2003), which explains the male infertility in *Cnnm4*-deficient mice. Incomplete Ca^{2+} influx observed in *Cnnm4*-deficient sperm might be sufficient for maintaining sperm motility to some extent, but the full Ca^{2+} influx seems to be required for hyperactivation. It

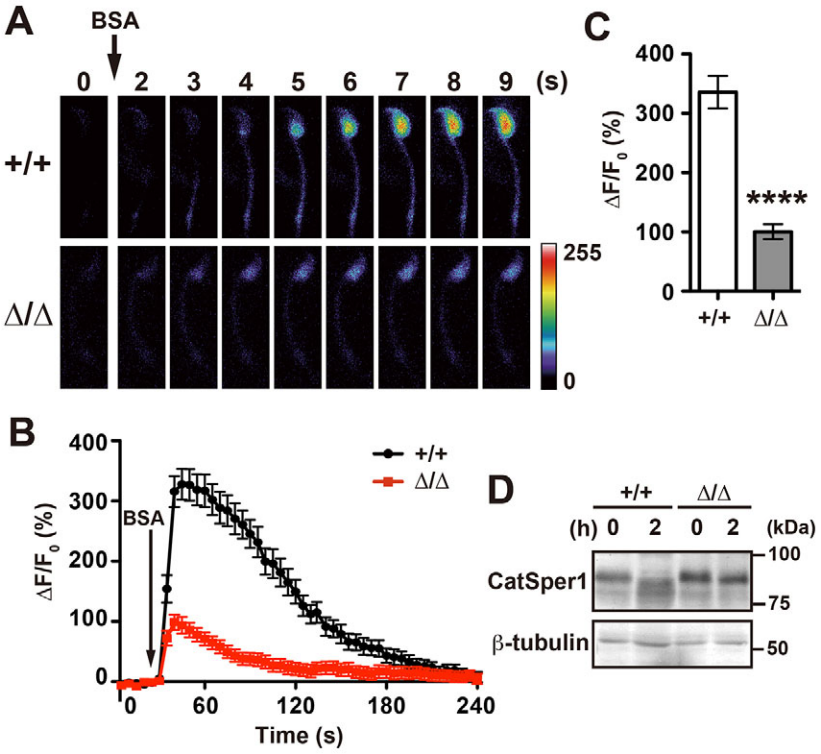

Fig. 6. *Cnnm4*-deficient sperm show impaired Ca^{2+} influx. (A) Time-lapse images of the fluorescence of Ca^{2+} indicator Fluo-4 in sperm treated with BSA (5 mg/ml) are shown in pseudocolor. The timing of BSA application is shown with an arrow. (B) Fluorescence changes ($\Delta F/F_0$) in the sperm head. The timing of BSA application is shown with an arrow. Data are expressed as mean±s.e.m. (n=50 from 4 mice for each genotype). (C) Peak $\Delta F/F_0$ ratio in the head region. Data are expressed as mean±s.e.m. (n=50 from 4 mice for each genotype). ****P<0.0001 (two-tailed Student's t-test). (D) Sperm were incubated in the TYH medium for the indicated time. Lysates of sperm were immunoblotted with the indicated antibodies.

Journal of Cell Science (2016) 129, 1940-1949 doi:10.1242/jcs.182220

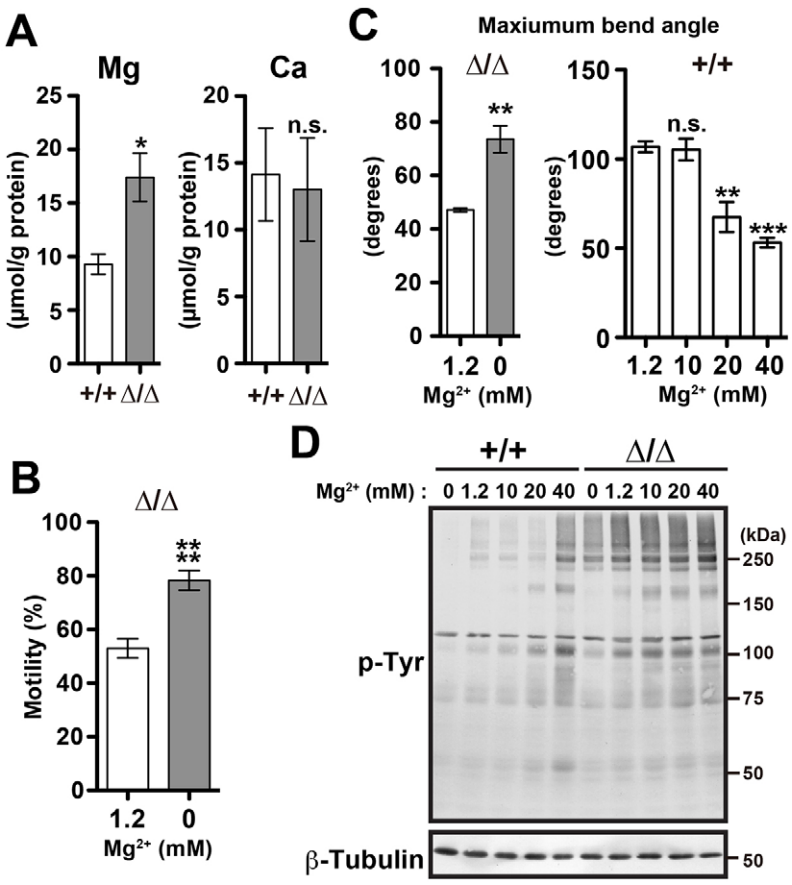

Fig. 7. Mg^{2+} regulates sperm motility and hyperactivation. (A) Sperm lysates were subjected to elemental analysis using ICP-MS. Data are expressed as mean±s.e.m. (n=4). *P<0.05; n.s., not significant (two-tailed Student's t-test). (B) *Cnnm4*-deficient sperm were incubated in the Mg^{2+}-free TYH medium for 10 min and were transferred to Mg^{2+}-free or normal TYH medium, followed by incubation for 110 min. Their percentage motility was measured. Data are expressed as mean±s.e.m. Four independent experiments were performed. ****P<0.0001 (chi-squared test). (C) *Cnnm4*-deficient (left) and wild-type (right) sperm were incubated in the Mg^{2+}-free medium for 10 min and were transferred to the medium containing the indicated concentrations of Mg^{2+} for 110 min. Their maximum bend angles of the mid-piece were measured. Data are expressed as mean ±s.e.m. Three (left) or four (right) independent experiments were performed. **P<0.01, ***P<0.001; n.s., not significant (two-tailed Student's t-test, left; one-way ANOVA with Tukey's multiple comparison test, right). (D) Sperm were incubated in the medium containing the indicated concentrations of Mg^{2+} for 2 h. Sperm lysates were immunoblotted with the indicated antibodies.

remains elusive to what extent the CatSper channel is responsible for the defect in *Cnnm4*-deficient sperm. We should also consider the possibility that CNNM4 regulates sperm Ca^{2+} homeostasis in a manner independent of the CatSper channel. Future studies should investigate the possible functional relationship between the intrinsic Mg^{2+} efflux activity of CNNMs and Ca^{2+} homeostasis.

MATERIALS AND METHODS

Generation of *Cnnm4*-deficient mice

Cnnm4-deficient mice lacking exons 2–5 of *Cnnm4* were generated by mating $Cnnm4^{-/-}$ mice produced in the previous study (Yamazaki et al., 2013) with transgenic mice expressing Cre recombinase under the control of a ubiquitous CAG promoter (Funato et al., 2014). The resulting $Cnnm4^{+/\Delta}$ offspring lacking a neomycin-resistance gene and exons 2–5 of *Cnnm4* were bred to homozygosity.

Specific disruption of *Cnnm4* in male germ cells was achieved using the following 3-step procedure: (1) $Cnnm4^{+/\Delta}$;*Stra8-Cre* mice were generated by mating $Cnnm4^{+/\Delta}$ mice with transgenic mice expressing Cre recombinase under the control of the germ-cell-specific *Stra8* promoter (Tokuhiro et al., 2015). (2) To generate the allele $Cnnm4^{flox}$, in which exons 2–5 of *Cnnm4* can be deleted in the presence of Cre recombinase, $Cnnm4^{-/-}$ mice were mated with transgenic mice expressing optimized Flp recombinase (Flpo) under the control of a ubiquitous CAG promoter produced as explained in the next paragraph. (3) The resulting $Cnnm4^{+/flox}$ offspring were mated with the $Cnnm4^{+/\Delta}$;*Stra8-Cre* mice to generate $Cnnm4^{flox/\Delta}$;*Stra8-Cre* mice. These $Cnnm4^{flox/\Delta}$;*Stra8-Cre* mice were used for analyses.

Flpo-expressing mice were generated as follows: the cDNA encoding Flpo was obtained by performing PCR with pPGKFLPobpA (#13793, Addgene) as the template. This cDNA was inserted into pCAG1.1 vector containing the CAG promoter and a rabbit globin polyA signal (Ikawa et al., 2001). A transgenic mouse line was produced by microinjecting the transgene into fertilized eggs from B6D2F1 crosses.

Genotyping PCR was performed using the following primers: 5F, 5′-ATGTGGGCAGCTGCTAGACT-3′; 5R, 5′-CCTGTCACAAGAAGGGGAAA-3′; 5R2, 5′-AGACCTTGGGACCACCTCAT-3′; LF, 5′-CCCCCTGAACCTGAAACATA-3′; LR, 5′-CGGGACATCCTAGGTGTGGA-3′; 3F, 5′-TAACTGTTGGAAGGCT-3′; and 3R, 5′-AGGCAGGGGCTCCCTTTCAT-3′. The positions of these primers are shown in Figs S1A and S3A. Presence of *Cre*, *Flpo*, and *Neo* was examined by performing PCR with the following primer sets: *Cre*, 5′-GTTTCACTGGTTATGCGGCGG-3′ and 5′-TTCCAGGGCGCGAGTTGATAG-3′; *Flpo*, 5′-GCAACGTGCTGGTTGTTGTGCTGTCTCATC-3′ and 5′-ACTCGAGTCAGACCGCCTGTTGATGTAGCTG-3′; and *Neo*, 5′-ATGATTGAACAAGATGGATT-3′ and 5′-AGCCGCGCTGCCTCGTCCTG-3′. For genotyping of juvenile mice, genomic DNAs isolated from tails were used as a template.

Mice were treated appropriately in accordance with the guidelines for proper conduct of animal experiments (issued by the Science Council of Japan) to ameliorate their suffering. This study was approved by the institutional review board of Osaka University.

Antibodies and reagents

Rabbit anti-CNNM4 antibody (Yamazaki et al., 2013) and rat anti-IZUMO1 antibody (Ikawa et al., 2011) were produced as described in the indicated studies. We used the following commercially available primary antibodies: anti-phosphotyrosine antibody (1:2000, 05-321; Merck Millipore); anti-BASIGIN, anti-CatSper1, and anti-Tom20 antibody (1:2000, sc-9757; 1:1000, sc-21180; and 1:200, sc-17764, respectively; Santa Cruz Biotechnology); anti-β-tubulin antibody (1:5000, T4026; Sigma-Aldrich). We used the following commercially available secondary antibodies: Alexa-Fluor-488-conjugated anti-rabbit- and anti-mouse-IgG antibodies (Life Technologies) for immunofluorescence staining and alkaline phosphatase-conjugated anti-rabbit-, anti-mouse-, anti-rat- and anti-goat-IgG antibodies (Promega) for immunoblotting analyses. We used the following commercially available reagents: 3-aminopropyltriethoxysilane, A23187, collagenase, laminin (Sigma-Aldrich); Fluo-4AM (Dojindo); pluronic

F-127 and lipid-rich BSA (AlbuMAX, for sperm incubation; Life Technologies); and hyaluronidase (Vitrolife).

Fertility test

Male fertility was analyzed using 2- to 3-month-old male mice. Each male mouse was caged with two 2-month-old B6D2F1 females (Japan SLC) for 3 months. In total, four or five male mice were examined for each genotype. Copulatory behavior was checked by examining the vaginal plug every morning. Pregnancy rates are expressed as the ratio of the number of pregnant female mice to the number of plug-positive female mice.

Human sperm preparation

All the experiments using human samples were approved by the Ethics Committee of the Research Institute for Microbial Diseases, Osaka University, Japan. Human semen samples were obtained from fertile donors. Human sperm were collected by the swim-up method (Miyata et al., 2015), and then solubilized in lysis buffer (40 mM Tris-HCl pH 7.5, 150 mM NaCl, and 0.5% Triton X-100). The solution was centrifuged at 17,400 ***g*** for 10 min, and the supernatant was subjected to immunoblotting.

Immunofluorescence microscopy

Sperm from the cauda epididymis were released into phosphate-buffered saline (PBS) and were collected. For staining CNNM4, they were mounted on glass slides coated with 3-aminopropyltriethoxysilane, air-dried, fixed with PBS containing 3.7% formaldehyde for 15 min, and incubated in ice-cold methanol for 5 min at room temperature. For staining of phosphorylated tyrosine, sperm were fixed with PBS containing 4% paraformaldehyde for 10 min and then mounted. The specimens were permeabilized with 0.5% Triton X-100 in PBS for 5 min. After blocking with PBS containing 3% fetal bovine serum and 10% BSA (blocking buffer) for 1 h at room temperature, the specimens were incubated overnight at 4°C with specific primary antibodies diluted in blocking buffer. After washing with PBS, the specimens were incubated for 1 h at room temperature with Alexa-Fluor-488-conjugated anti-rabbit- or anti-mouse-IgG antibody diluted in blocking buffer. The specimens were then mounted with PermaFluor aqueous mounting medium (Thermo Scientific) and were examined under a confocal laser scanning microscope (FluoView FV1000; Olympus).

Antigen absorption

Glutathione S-transferase (GST)-tagged CNNM4 proteins (amino acids 546–775) were expressed in Sf9 cells and purified with glutathione beads (GE Healthcare). The purified proteins (GST-antigen) were used in antigen absorption experiments with the anti-CNNM4 antibody. The anti-CNNM4 antibody (200 ng) was incubated with GST (12 µg) or GST antigen (4 µg) in blocking buffer for 2 h, and then subjected to immunostaining.

β-Galactosidase staining

The testis and epididymis were dissected from 3- to 5-month-old mice, embedded in a Tissue-Tek O.C.T. compound (Sakura Finetek), frozen in liquid nitrogen and sliced into 10-µm-thick sections by using a cryostat (CM1900; Leica). Cryosections were fixed with PBS containing 0.4% glutaraldehyde for 10 min at room temperature. The fixed sections were stained with PBS containing 1 mg/ml X-gal, 5 mM $K_3[Fe(CN)_6]$, 5 mM $K_4[Fe(CN)_6]$, 1 mM $MgCl_2$ and 0.01% Triton X-100, counterstained with Neutral Red (0.5% Neutral Red, 3.2 mM acetic acid, and 4.8 mM sodium acetate) and examined under a microscope (BX41 equipped with a DP73 camera; Olympus).

H&E staining

The testis and epididymis of 3-month-old mice were dissected, and their cryosections were prepared as described above. The sections were fixed with PBS containing 3.7% formaldehyde for 10 min at room temperature, stained with Meyer's hematoxylin (Wako) and 0.1% eosin Y (Wako), and observed under a microscope (BX41 equipped with a DP73 camera).

Separation of sperm heads and tails

The heads and tails of sperm were separated as described previously (Zalata et al., 1998). Briefly, cauda epididymal sperm were suspended in PBS, and their heads and tails were separated by sonication for 15 s in a sonicator (VP-5S; Taitec). The mixture was centrifuged at 5000 ***g*** for 5 min. The pellet was resuspended in 90% Percoll (GE Healthcare) in PBS and was centrifuged at 15,000 ***g*** for 15 min. Centrifugation resulted in the fractionation of sperm heads and tails at the bottom and top of the Percoll solution, respectively. Each fraction was diluted in PBS and was centrifuged at 9000 ***g*** for 5 min to precipitate the sperm heads and tails. After washing twice with PBS, the samples were used for immunoblotting analyses.

IVF

IVF was performed as described previously (Tokuhiro et al., 2012). Briefly, cauda epididymal sperm were collected and were incubated in TYH medium (119 mM NaCl, 4.8 mM KCl, 1.2 mM $MgSO_4$, 25 mM $NaHCO_3$, and 4 mg/ml BSA) for 2 h at 37°C for capacitation. Eggs collected from superovulated females at 14 h after injecting human chorionic gonadotropin (Aska Pharmaceutical) were treated with 330 µg/ml hyaluronidase for 10 min to remove the cumulus cells (zona-pellucida-intact eggs) or with 1 mg/ml collagenase for 10 min to remove zona pellucida (zona-pellucida-free eggs). The capacitated sperm were added to a drop of the TYH medium containing zona-pellucida-intact or zona-pellucida-free eggs at a final density of 2×10^5 or 4×10^4 sperm/ml, respectively. When IVF was performed using zona-pellucida-intact eggs, two-celled embryos were counted on the next day. When IVF was performed using zona-pellucida-free eggs, pronuclear formation was observed 8 h after co-incubation.

Sperm count

Sperm were collected from the proximal vas deferens (1 cm from the cauda epididymis) by squeezing with forceps and were suspended in the TYH medium. The sperm were then cooled for 30 min at 4°C to arrest their movement, and their number was counted using a hemocytometer.

Sperm motility test

CASA was performed to determine the motility of cauda epididymal sperm. Sperm were incubated in the TYH medium at 37°C, and their motility was assessed using a CEROS Sperm Analyzer (Hamilton Thorne Research). The percentage of motile sperm and their path, linear and track velocities were determined.

Waveform analysis

Cauda epididymal sperm were incubated in the TYH medium for 5 min or 2 h at 37°C and were placed into a counting chamber (20-µm depth; Leja). Flagellar movement of these sperm was observed for ∼2 s under a microscope (BX-53; Olympus), and negative phase-contrast images were obtained at 200 Hz with a CMOS camera (HAS-L1; Direct) by using the attached software. Flagellar movement was quantitatively analyzed by placing the sperm on a glass-based dish (IWAKI). Live sperm were observed under an inverted microscope (IB81; Olympus), and phase-contrast images were obtained at 100 Hz with a CMOS camera (ORCA-Flash4.0; Hamamatsu Photonics) by using MetaMorph software (Molecular Devices). Bend angle of the sperm mid-piece was measured manually by using ImageJ software (NIH). Each image obtained during 1 complete beat cycle (∼200 ms) was analyzed, and the maximum bend angle was determined for each sperm.

Ca^{2+} imaging

Cauda epididymal sperm were released into BSA-free TYH medium, and were loaded with 10 µM Fluo-4AM and 0.05% pluronic F-127 for 1 h at 37°C. The sperm were washed, resuspended in BSA-free TYH medium, and placed on a laminin-coated glass-based dish. After 10 min, the evenly loaded sperm were observed under an inverted microscope (IX81; Olympus) at room temperature. Fluorescence images (excitation at 470–490 nm and emission at 505–545 nm) were obtained every 1 s with a CMOS camera (ORCA-Flash4.0; Hamamatsu Photonics) by using the MetaMorph software 1 min before applying 5 mg/ml BSA. Fluorescence signal intensities of sperm heads were measured manually by using ImageJ software. Data are presented as the ratio of the change in fluorescence signal intensity (ΔF) compared with baseline signal intensity (F_0) determined by averaging ten frames before BSA application, as described previously (Xia and Ren, 2009a).

ICP-MS

Sperm from the cauda epididymis were lysed in 40% HNO_3 at 95°C for 2 h. The lysates were diluted ten times with double-distilled H_2O and then subjected to elementary analysis with ICP-MS 7700x (Agilent), according to the manufacturer's instructions. The Mg^{2+} and Ca^{2+} levels were normalized to total protein levels, which were determined using the BCA assay kit (Thermo Scientific).

Manipulation of extracellular Mg^{2+}

To change the concentration of Mg^{2+} in the incubation medium, we prepared Mg^{2+}-free (119 mM NaCl, 4.8 mM KCl, 25 mM $NaHCO_3$, and 4 mg/ml BSA) and 80 mM Mg^{2+}-containing (4.8 mM KCl, 80 mM $MgCl_2$, 25 mM $NaHCO_3$, and 4 mg/ml BSA) media. To keep the osmolarity constant, NaCl was excluded from the latter medium. In Fig. 7, to prepare the media containing various concentration of Mg^{2+}, these two media were mixed at the appropriate ratio.

Statistical analysis

Statistical analyses were performed using Prism 5 (GraphPad). Student's two-tailed *t*-tests were used to calculate the *P* values of most data analyses. A chi-squared test was used to calculate *P* values in Figs 1A, left, 3D and 7B. Tukey's multiple comparison test was used after one-way analysis of variance to calculate *P* values in Figs 4D and 7C, right, and Fig. S4D.

Acknowledgements

We thank Ms Nao Arita for technical assistance.

Competing interests

The authors declare no competing or financial interests.

Author contributions

H. Miki conceived the study design and wrote the manuscript, with contributions from D.Y. D.Y. performed most of the experiments, with contributions from H. Miyata, Y. Funato, Y. Fujihara and M.I. H. Miyata and M.I. performed IVF experiments. All the authors read and approved the final manuscript.

Funding

This work was supported by the Japan Society for the Promotion of Science (KAKENHI) [grant numbers 26430113 to D.Y., 26460364 to Y. Funato, 26291042 to H. Miki and 26111007 to H. Miki].

Supplementary information

Supplementary information available online at
http://jcs.biologists.org/lookup/suppl/doi:10.1242/jcs.182220/-/DC1

References

Austin, C. R. (1951). Observations on the penetration of the sperm in the mammalian egg. *Aust. J. Sci. Res. B* **4**, 581-596.

Austin, C. R. (1952). The 'capacitation' of the mammalian sperm. *Nature* **170**, 326.

Carlson, A. E., Westenbroek, R. E., Quill, T., Ren, D., Clapham, D. E., Hille, B., Garbers, D. L. and Babcock, D. F. (2003). CatSper1 required for evoked Ca^{2+} entry and control of flagellar function in sperm. *Proc. Natl. Acad. Sci. USA* **100**, 14864-14868.

Carlson, A. E., Quill, T. A., Westenbroek, R. E., Schuh, S. M., Hille, B. and Babcock, D. F. (2005). Identical phenotypes of CatSper1 and CatSper2 null sperm. *J. Biol. Chem.* **280**, 32238-32244.

Chang, M. C. (1951). Fertilizing capacity of spermatozoa deposited into the fallopian tubes. *Nature* **168**, 697-698.

Chen, Y., Cann, M. J., Litvin, T. N., Iourgenko, V., Sinclair, M. L., Levin, L. R. and Buck, J. (2000). Soluble adenylyl cyclase as an evolutionarily conserved bicarbonate sensor. *Science* **289**, 625-628.

Chung, J.-J., Navarro, B., Krapivinsky, G., Krapivinsky, L. and Clapham, D. E. (2011). A novel gene required for male fertility and functional CATSPER channel formation in spermatozoa. *Nat. Commun.* **2**, 153.

Chung, J.-J., Shim, S.-H., Everley, R. A., Gygi, S. P., Zhuang, X. and Clapham, D. E. (2014). Structurally distinct Ca^{2+} signaling domains of sperm flagella orchestrate tyrosine phosphorylation and motility. *Cell* **157**, 808-822.

Darszon, A., Nishigaki, T., Beltran, C. and Treviño, C. L. (2011). Calcium channels in the development, maturation, and function of spermatozoa. *Physiol. Rev.* **91**, 1305-1355.

de Baaij, J. H. F., Stuiver, M., Meij, I. C., Lainez, S., Kopplin, K., Venselaar, H., Müller, D., Bindels, R. J. M. and Hoenderop, J. G. J. (2012). Membrane topology and intracellular processing of cyclin M2 (CNNM2). *J. Biol. Chem.* **287**, 13644-13655.

Demarco, I. A., Espinosa, F., Edwards, J., Sosnik, J., De la Vega-Beltran, J. L., Hockensmith, J. W., Kopf, G. S., Darszon, A. and Visconti, P. E. (2003). Involvement of a Na^+/HCO_3^- cotransporter in mouse sperm capacitation. *J. Biol. Chem.* **278**, 7001-7009.

Espinosa, F., López-González, I., Muñoz-Garay, C., Felix, R., De la Vega-Beltrán, J. L., Kopf, G. S., Visconti, P. E. and Darszon, A. (2000). Dual regulation of the T-type Ca(2+) current by serum albumin and beta-estradiol in mammalian spermatogenic cells. *FEBS Lett.* **475**, 251-256.

Funato, Y., Yamazaki, D., Mizukami, S., Du, L., Kikuchi, K. and Miki, H. (2014). Membrane protein CNNM4-dependent Mg^{2+} efflux suppresses tumor progression. *J. Clin. Invest.* **124**, 5398-5410.

Hirata, Y., Funato, Y., Takano, Y. and Miki, H. (2014). Mg^{2+}-dependent interactions of ATP with the cystathionine-β-synthase (CBS) domains of a magnesium transporter. *J. Biol. Chem.* **289**, 14731-14739.

Ikawa, M., Nakanishi, T., Yamada, S., Wada, I., Kominami, K., Tanaka, H., Nozaki, M., Nishimune, Y. and Okabe, M. (2001). Calmegin is required for fertilin alpha/beta heterodimerization and sperm fertility. *Dev. Biol.* **240**, 254-261.

Ikawa, M., Tokuhiro, K., Yamaguchi, R., Benham, A. M., Tamura, T., Wada, I., Satouh, Y., Inoue, N. and Okabe, M. (2011). Calsperin is a testis-specific chaperone required for sperm fertility. *J. Biol. Chem.* **286**, 5639-5646.

Lishko, P. V., Kirichok, Y., Ren, D., Navarro, B., Chung, J.-J. and Clapham, D. E. (2012). The control of male fertility by spermatozoan ion channels. *Annu. Rev. Physiol.* **74**, 453-475.

Liu, J., Xia, J., Cho, K.-H., Clapham, D. E. and Ren, D. (2007). CatSperbeta, a novel transmembrane protein in the CatSper channel complex. *J. Biol. Chem.* **282**, 18945-18952.

Miyata, H., Satouh, Y., Mashiko, D., Muto, M., Nozawa, K., Shiba, K., Fujihara, Y., Isotani, A., Inaba, K. and Ikawa, M. (2015). Sperm calcineurin inhibition prevents mouse fertility with implications for male contraceptive. *Science* **350**, 442-445.

Osheroff, J. E., Visconti, P. E., Valenzuela, J. P., Travis, A. J., Alvarez, J. and Kopf, G. S. (1999). Regulation of human sperm capacitation by a cholesterol efflux-stimulated signal transduction pathway leading to protein kinase A-mediated up-regulation of protein tyrosine phosphorylation. *Mol. Hum. Reprod.* **5**, 1017-1026.

Qi, H., Moran, M. M., Navarro, B., Chong, J. A., Krapivinsky, G., Krapivinsky, L., Kirichok, Y., Ramsey, I. S., Quill, T. A. and Clapham, D. E. (2007). All four CatSper ion channel proteins are required for male fertility and sperm cell hyperactivated motility. *Proc. Natl. Acad. Sci. USA* **104**, 1219-1223.

Quill, T. A., Sugden, S. A., Rossi, K. L., Doolittle, L. K., Hammer, R. E. and Garbers, D. L. (2003). Hyperactivated sperm motility driven by CatSper2 is required for fertilization. *Proc. Natl. Acad. Sci. USA* **100**, 14869-14874.

Ren, D. and Xia, J. (2010). Calcium signaling through CatSper channels in mammalian fertilization. *Physiology* **25**, 165-175.

Ren, D., Navarro, B., Perez, G., Jackson, A. C., Hsu, S., Shi, Q., Tilly, J. L. and Clapham, D. E. (2001). A sperm ion channel required for sperm motility and male fertility. *Nature* **413**, 603-609.

Sadate-Ngatchou, P. I., Payne, C. J., Dearth, A. T. and Braun, R. E. (2008). Cre recombinase activity specific to postnatal, premeiotic male germ cells in transgenic mice. *Genesis* **46**, 738-742.

Santi, C. M., Santos, T., Hernández-Cruz, A. and Darszon, A. (1998). Properties of a novel pH-dependent Ca^{2+} permeation pathway present in male germ cells with possible roles in spermatogenesis and mature sperm function. *J. Gen. Physiol.* **112**, 33-53.

Suarez, S. S. (2008). Control of hyperactivation in sperm. *Hum. Reprod. Update* **14**, 647-657.

Tateno, H., Krapf, D., Hino, T., Sánchez-Cárdenas, C., Darszon, A., Yanagimachi, R. and Visconti, P. E. (2013). Ca^{2+} ionophore A23187 can make mouse spermatozoa capable of fertilizing in vitro without activation of cAMP-dependent phosphorylation pathways. *Proc. Natl. Acad. Sci. USA* **110**, 18543-18548.

Tokuhiro, K., Ikawa, M., Benham, A. M. and Okabe, M. (2012). Protein disulfide isomerase homolog PDILT is required for quality control of sperm membrane protein ADAM3 and male fertility. *Proc. Natl. Acad. Sci. USA* **109**, 3850-3855.

Tokuhiro, K., Satouh, Y., Nozawa, K., Isotani, A., Fujihara, Y., Hirashima, Y., Matsumura, H., Takumi, K., Miyano, T., Okabe, M. et al. (2015). Calreticulin is required for development of the cumulus oocyte complex and female fertility. *Sci. Rep.* **5**, 14254.

Visconti, P. E., Moore, G. D., Bailey, J. L., Leclerc, P., Connors, S. A., Pan, D., Olds-Clarke, P. and Kopf, G. S. (1995). Capacitation of mouse spermatozoa. II. Protein tyrosine phosphorylation and capacitation are regulated by a cAMP-dependent pathway. *Development* **121**, 1139-1150.

Visconti, P. E., Ning, X., Fornés, M. W., Alvarez, J. G., Stein, P., Connors, S. A. and Kopf, G. S. (1999). Cholesterol efflux-mediated signal transduction in mammalian sperm: cholesterol release signals an increase in protein tyrosine phosphorylation during mouse sperm capacitation. *Dev. Biol.* **214**, 429-443.

Wang, C.-Y., Shi, J.-D., Yang, P., Kumar, P. G., Li, Q.-Z., Run, Q.-Z., Su, Y.-C., Scott, H. S., Kao, K.-J. and She, J.-X. (2003). Molecular cloning and characterization of a novel gene family of four ancient conserved domain proteins (ACDP). *Gene* **306**, 37-44.

Wang, C.-Y., Yang, P., Shi, J.-D., Purohit, S., Guo, D., An, H., Gu, J.-G., Ling, J., Dong, Z. and She, J.-X. (2004). Molecular cloning and characterization of the mouse Acdp gene family. *BMC Genomics* **5**, 7.

Wang, H., Liu, J., Cho, K.-H. and Ren, D. (2009). A novel, single, transmembrane protein CATSPERG is associated with CATSPER1 channel protein. *Biol. Reprod.* **81**, 539-544.

Wortzman-Show, G. B., Kurokawa, M., Fissore, R. A. and Evans, J. P. (2007). Calcium and sperm components in the establishment of the membrane block to polyspermy: studies of ICSI and activation with sperm factor. *Mol. Hum. Reprod.* **13**, 557-565.

Xia, J. and Ren, D. (2009a). The BSA-induced Ca^{2+} influx during sperm capacitation is CATSPER channel-dependent. *Reprod. Biol. Endocrinol.* **7**, 119.

Xia, J. and Ren, D. (2009b). Egg coat proteins activate calcium entry into mouse sperm via CATSPER channels. *Biol. Reprod.* **80**, 1092-1098.

Xia, J., Reigada, D., Mitchell, C. H. and Ren, D. (2007). CATSPER channel-mediated Ca^{2+} entry into mouse sperm triggers a tail-to-head propagation. *Biol. Reprod.* **77**, 551-559.

Yamazaki, D., Funato, Y., Miura, J., Sato, S., Toyosawa, S., Furutani, K., Kurachi, Y., Omori, Y., Furukawa, T., Tsuda, T. et al. (2013). Basolateral Mg^{2+} extrusion via CNNM4 mediates transcellular Mg^{2+} transport across epithelia: a mouse model. *PLoS Genet.* **9**, e1003983.

Yanagimachi, R. (1994). Mammalian fertilization. In *The Physiology of Reproduction*, 2nd edn (ed. E. Knobile and J. D. Neill), pp. 189-317. New York: Raven Press.

Zalata, A. A., Christophe, A. B., Depuydt, C. E., Schoonjans, F. and Comhaire, F. H. (1998). The fatty acid composition of phospholipids of spermatozoa from infertile patients. *Mol. Hum. Reprod.* **4**, 111-118.

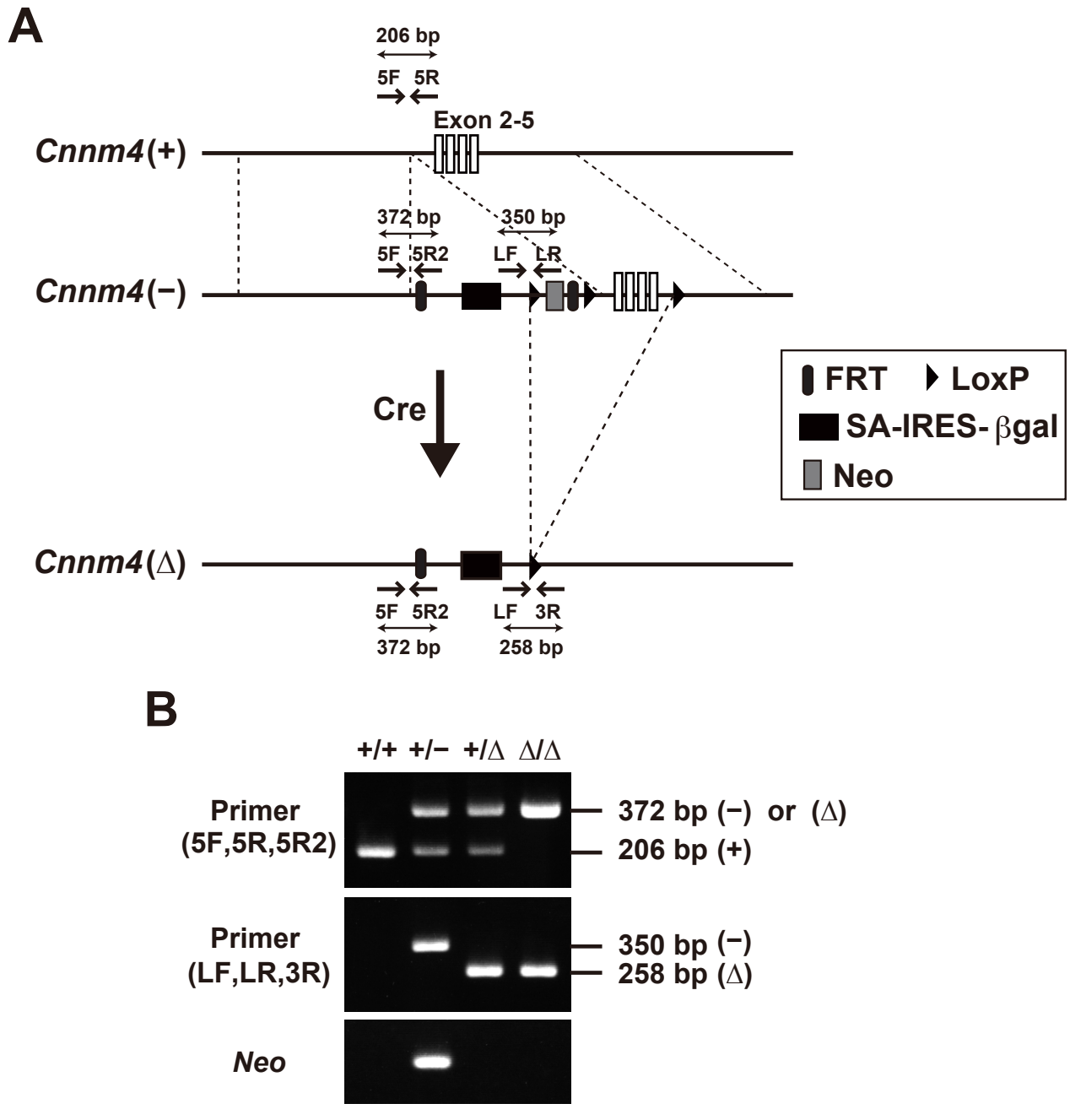

Fig. S1. Generation of *Cnnm4*$^{\Delta/\Delta}$ mice. (A) Targeting strategy. βgal, β-galactosidase gene; FRT, Flp recombination target; IRES, internal ribosomal entry site; loxP, locus of crossing over P1; Neo, neomycin resistance gene; SA, splice acceptor. (B) Genotyping PCR was performed using genomic DNA extracted from mice tails and oligonucleotide primers shown in (A).

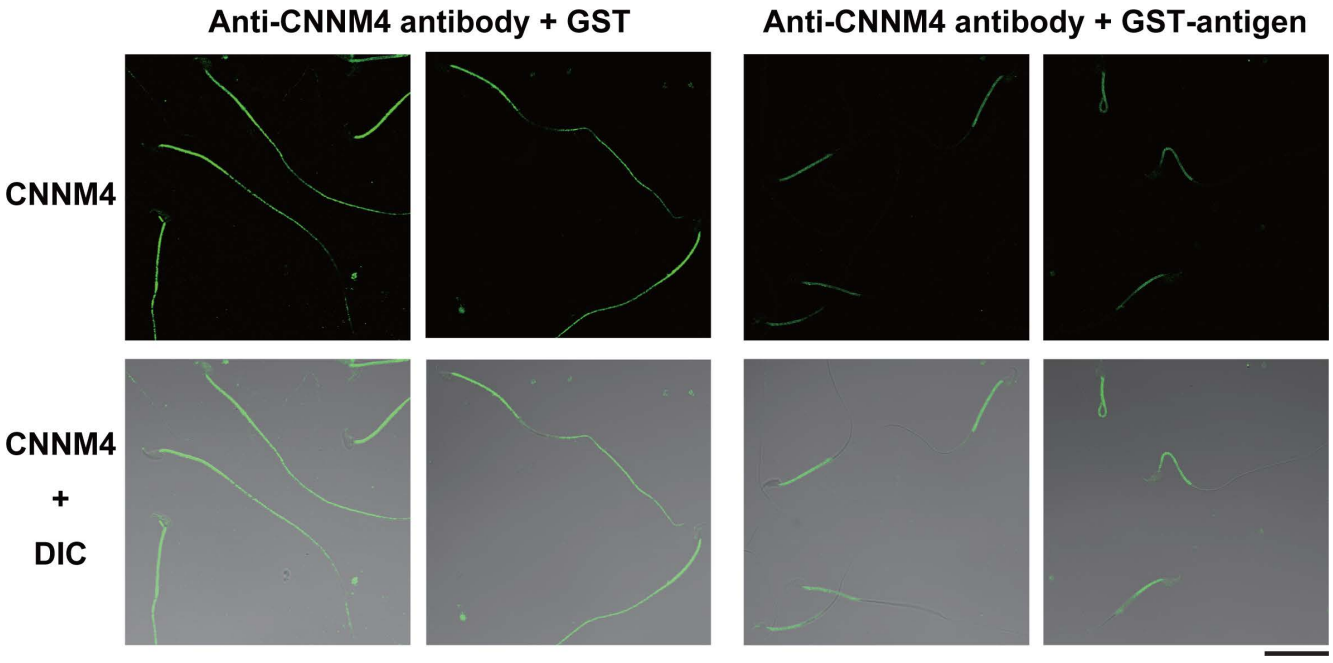

Fig. S2. Antigen absorption test for anti-CNNM4 antibody on immunostaining. Wild-type sperm were subjected to immunofluorescence staining using anti-CNNM4 antibodies, which were pre-incubated with GST or GST-antigen. Differential interference contrast images are also indicated. Bar, 20 μm.

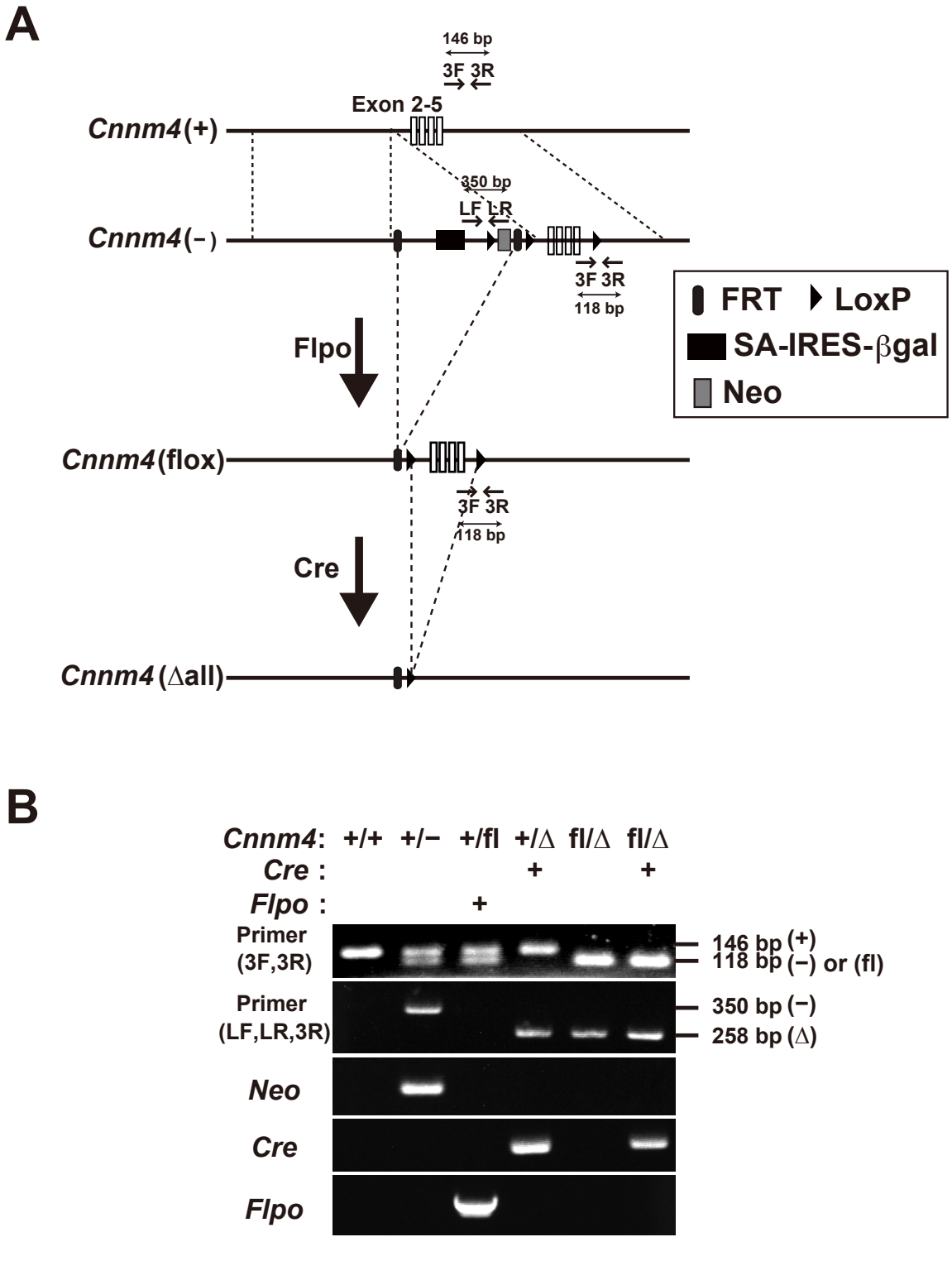

Fig. S3. Generation of *Cnnm4*$^{flox/\Delta}$;*Stra8-Cre* mice. (A) Targeting strategy. βgal, β-galactosidase gene; FRT, Flp recombination target; IRES, internal ribosomal entry site; loxP, locus of crossing over P1; Neo, neomycin resistance gene; SA, splice acceptor. (B) Genotyping PCR was performed using genomic DNA extracted from mice tails and oligonucleotide primers shown in (A).

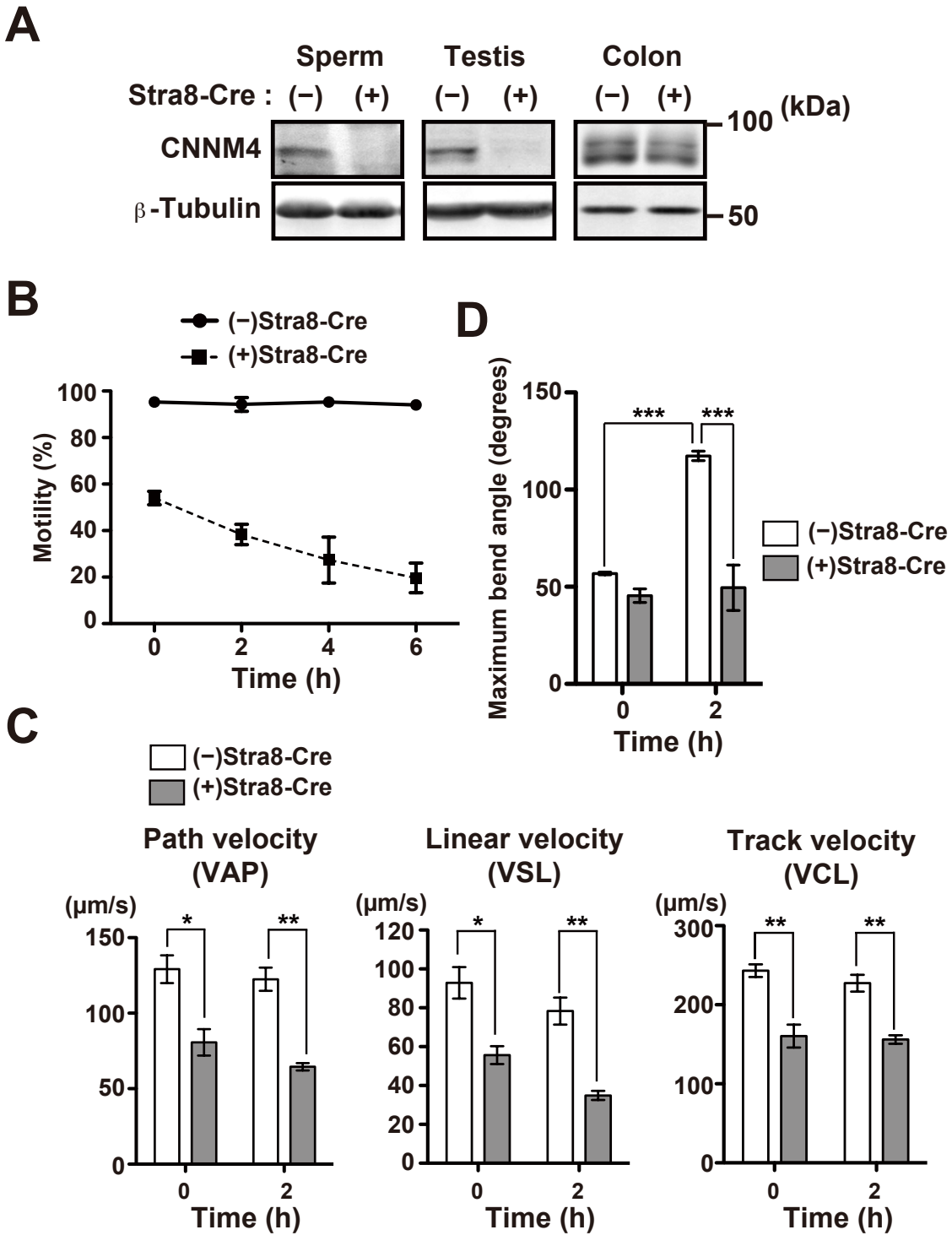

Fig. S4. Germ cell-specific deletion of *Cnnm4*. (A) Lysates of sperm, testis, and colon obtained from 3-month-old *Cnnm4*$^{flox/\Delta}$ and *Cnnm4*$^{flox/\Delta}$;*Stra8-Cre* mice were immunoblotted with the indicated antibodies. (B) Sperm were incubated for the indicated time, and percentage motility was measured using CASA. Data are expressed as mean ± s.e.m. Three independent experiments were performed. (C) Sperm were incubated for the indicated time, and their path, linear, and track velocities were measured using CASA. Data are expressed as mean ± s.e.m. Three independent experiments were performed. *$p < 0.05$, **$p < 0.01$. (D) Sperm were incubated for the indicated time, and their maximum bend angles of the mid-piece were measured. In all, 60 sperm were analyzed from 3 mice of each genotype. Data are expressed as mean ± s.e.m of three independent experiments. ***$p < 0.001$.

Movie 1. Motility of sperm obtained from *Cnnm4*$^{+/+}$ mice before capacitation treatment.

Negative phase-contrast images obtained at 5-ms intervals were compiled into a single movie at 40 frames per/s.

Movie 2. Motility of sperm obtained from *Cnnm4*$^{\Delta/\Delta}$ mice before capacitation treatment.

The file was generated as Movie 1.

Movie 3. Motility of sperm obtained from *Cnnm4*$^{+/+}$ mice after capacitation treatment.

The file was generated as Movie 1.

Movie 4. Motility of sperm obtained from *Cnnm4*$^{\Delta/\Delta}$ mice after capacitation treatment.

The file was generated as Movie 1.